Fine structure of low-carbon steel after electrolytic plasma treatment

Lyaila Bayatanova, Ust-Kamenogorsk, Bauyrzhan Rakhadilov, Ust-Kamenogorsk, Sherzod Kurbanbekov, Turkistan, Mazhyn Skakov, Ust-Kamenogorsk, Kazakhstan, and Natalya Popova, Tomsk, Russia

Article Information

Correspondence Address
Sherzod Kurbanbekov
Khoja Akhmet Yassawi International Kazakh-Turkish University,
Turkistan, Kazakhstan
E-mail: sherzod.kurbanbekov@ayu.edu.kz

Keywords
Plasma, carbonitriding, steel, fine structure, phase

This work shows the results of research of the fine and dislocation structure of the transition layer of 18CrNi3Mo low-carbon steel after the influence of electrolytic plasma. Conducted research has shown that the modified steel layer, as a result of carbonitriding, was multiphase. Quantitative estimates were made for carbonitride $M_{23}(C,N)_6$ in various morphological components of α-martensite and on average by material in the transition layer of nitro-cemented steel. It was established that α-phase is tempered martensite after nitrocementation. Released martensite is represented by batch, or lath and lamellar low-temperature and high-temperature martensite. Inside the tempered martensitic crystals, lamellar cementite precipitates are simultaneously present, and residual austenite is found along the boundaries of the martensitic rails and plates of low-temperature martensite. It was determined that inside the crystals of all morphological components of α-martensite there are particles of carbonitride $M_{23}(C,N)_6$.

The important factor of sustainable development in industry is the widespread introduction of new highly efficient technologies that reduce energy consumption and have higher environmental and economic indicators. Such processes include the processing of metals and alloys by heating in an electrolytic plasma. Separately from traditional chemical heat treatment, environmentally safe aqueous solutions are used in electrolyte plasma processing, which are several times cheaper than toxic acid components [1].

Research has shown the effectiveness of using electrolytic-plasma processing for low-carbon structural steels. Materials from this class of steels after traditional chemical heat treatment have increased brittleness of the surface layer and a relatively low complex of properties of the core. The use of electrolytic-plasma treatment can significantly improve the properties of the surface layer, without reducing the properties of the core [2].

Applying the process of treatment by electrolytic plasma, the changes of structure-phase states and properties of the surface layer of the material occur due to the active influence of the electrolyte ions of the low-temperature plasma [3, 4]. So, the influence of treatment regimes in electrolytic plasma on the structural phase states and physicomechanical properties of the surface of low carbon steel is of great scientific and practical interest.

For the research of the modified layer structure of 18CrNi3Mo low carbon steel after heating in electrolytic plasma, a number of analytical studies were carried out using optical metallography and X-ray structural analysis [5]. However, in our opinion, much more in-depth and advanced results can be achieved by using "direct" experimental research methods, in particular, methods of transmission diffraction electron microscopy [6, 7]. The use of this method in studies of the boronation process [8, 9] showed a great potential for such an approach. This applies both to the methodical, practical, and to the fundamental side of the issue. Therefore, in the present work, the transmission electron microscopy method was developed and used to study the phase-structural state of the surface layer of 18CrNi3Mo steel after electrolytic-plasma carbonitriding. This made it possible to obtain fundamentally new and in-depth results, which made it possible to reveal the fundamental structural features of the nitro-cemented layer of 18CrNi3Mo steel.

The aim of this work was to study the fine and defective structure of the transition layer of 18CrNi3Mo steel after carbonitration in electrolyte plasma.

Experimental procedure

The research was conducted by the methods of electron diffraction microscopy on thin foils on the JEOL-2100 electron microscope using goniometric attachments at an accelerating voltage of 100 kV.

As a material, the study used samples of 18CrNi3Mo structural steel (0.16-0.18 % C; 3.3 % Ni; 0.9 % Cr; 0.51 % Mo; 0.44 % Mn; 0.34 %). Si; 0.05 % Al; 0.008 % S; 0.012 % P; 0.015 % N; 0.01 % O; 0.01 % H) (GOST 4543-71) after electrolytic-plasma carbonitriding (850 0C, 5 min.) [5].

Results and discussion

For research on treated steel using the TEM method, 2 sites were selected on the sample: 1) the subsurface layer (a detailed discussion of the results from this section

is described in [10]) and 2) 40 μm from the subsurface layer, i. e. in the transition zone. For this purpose, a plate with a thickness of 300 μm was cut on an electric-spark machine parallel to the nitro-cemented surface (measurements were made with a micrometer with an accuracy of ±0.01 μm).

Previously conducted X-ray research, the results of which are discussed in [11], showed that the structure of 18CrNi3Mo steel before processing consists of the α-phase based on iron. TEM results also confirmed this data [12]. The α-phase has a body-centered cubic (BCC) crystal lattice and can be solid solutions based on iron interstitial atoms (C, N, B, S, P and etc.) and substitutions (Si, Mn, Ni, Cr, Mo, V, W and etc.), simultaneously. In the case of the steel under study, the фа-phase is a solid solution for the substitution of Cr, Ni, and Mo and a solid solution for the introduction of carbon.

Carbonitriding has led to significant changes in the structure of steel. The α-phase is the released martensite. In turn of martensite is represented by batch, or rack, (see Figure 1), and lamellar, low-temperature (see Figure 2) and high-temperature (see Figure 3) martensite.

Batch (or lath) martensite is a structural formation consisting of a set of elongated crystals practically parallel to each other, forming a packet. Batch martensite is formed under the temperature $\gamma \rightarrow \alpha$ transformation of ~ 350 to 320 °C [13]. In the transition layer, the volume fraction of packet martensite is 40 %. The dislocation structure in martensitic rails is dense dislocation grids. On average, the scalar dislocation density is approximately $\rho = 5.3 \times 10^{10}$ cm^{-2}.

Lamellar low-temperature martensite consists of rather large, separately located, martensite crystals (plates) with a dislocation structure [14]. Lamellar martensite crystals are generally lens-shaped. The morphology and dislocation structure of this type of martensite has been studied in some detail in [15]. The temperature range of formation of low-temperature lamellar martensite is ~380 to 350 °C [13].

In the transition layer, the volume fraction of low-temperature plate martensite is 25 %. The dislocation structure in the plates also shows dislocation grids with an average scalar dislocation density of 4.1×10^{10} cm^{-2}.

Lamellar high-temperature martensite is composed of large, separately located martensite crystals (plates), often extending through the whole grain, as well as crystals of arbitrary shape, which do not have a

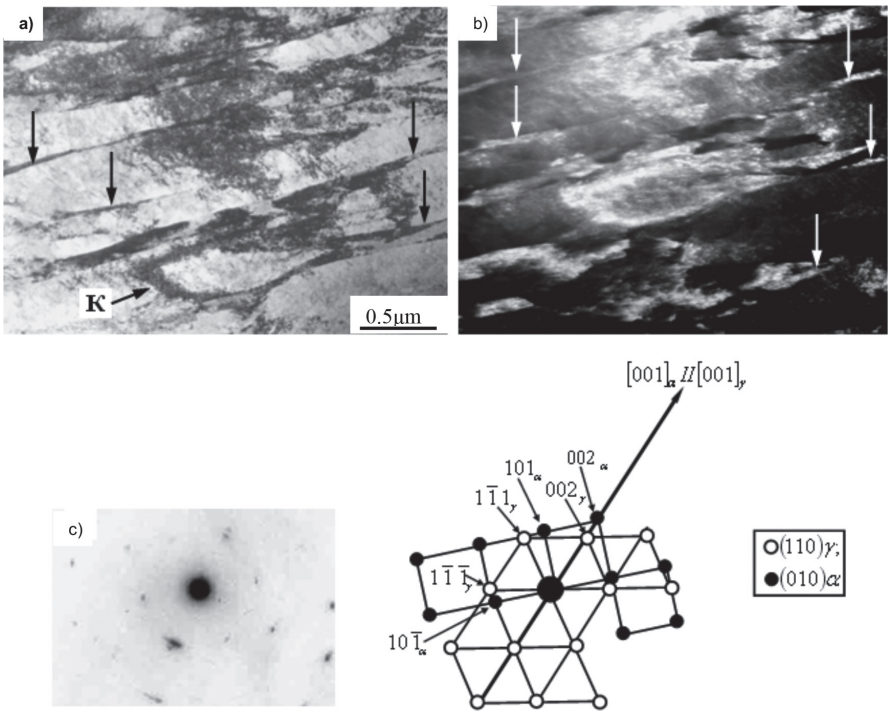

Figure 1: Intermediate layer of 18CrNi3Mo steel after carbonitriding, layers of residual austenite (γphase) along martensite rails boundaries, a) light-field image, interlayers of γphase as black arrows, b) dark-field image obtained in reflexes $[0\bar{1}\bar{1}]_\gamma + [10\bar{1}]_\alpha$, interlayers of γphase as white arrows, c) microdiffraction pattern, d) indicated scheme (the arrow indicates the coinciding directions $[001]_\gamma$ and [001]α, while $(110)_\gamma // (010)_\alpha$ is the Kurdyumov-Zaksa ratio), K: bending extinction contour

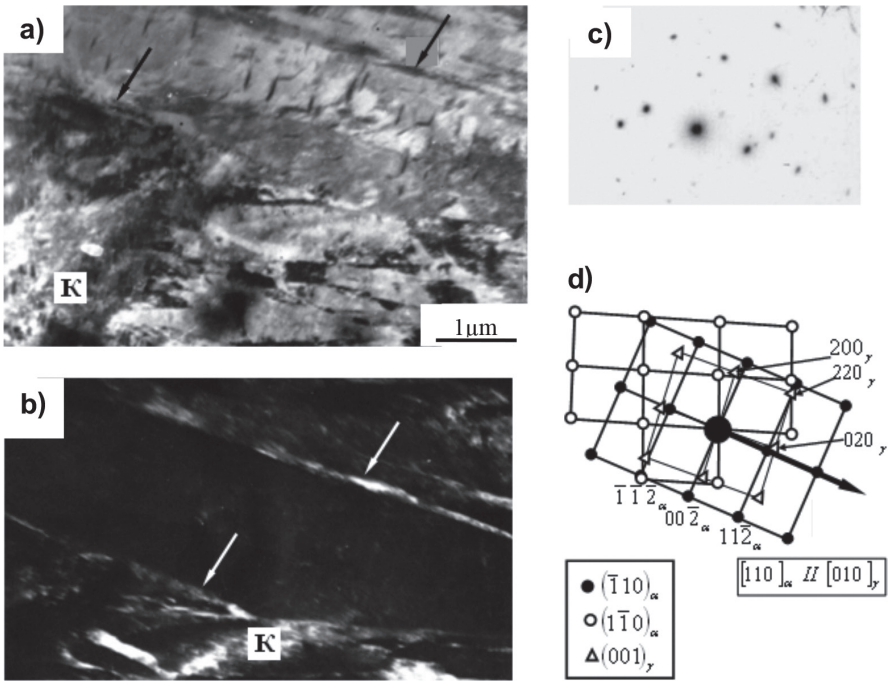

Figure 2: Intermediate layer of 18CrNi3Mo steel after carbonitriding, layers of residual austenite (γphase) along the boundaries of the low-temperature martensitic plate, a) light-field image,, interlayers of γphase as black arrows, b) dark-field image obtained in reflexes []α+[]γ, interlayers of γphase as white arrows, c) microdiffraction pattern, d) indexed circuit containing reflexes of the α- and γphases (the arrow indicates the matching directions $[110]_\alpha$ and $[010]_\gamma$ – the ratio Kurdyumov-Zaks), indication of the microdiffraction pattern (в) was carried out only for reflections related to the α- and γphases, K: bending extinction contour

clear cut and lack their own interfaces [13, 16]. The temperature range of formation of high-temperature lamellar martensite is ~400 to 380 °C [13]. The volume fraction of high-temperature martensite is 35 %. The dislocation structure is also reticulated. The average scalar dislocation density is ~3.5 × 10^{10} cm^{-2}.

All martensite is in the released condition. Inside the tempered martensitic crystals, there are, simultaneously, lamellar cementite precipitates of two or three orientations. The lattices of tempered м-martensite and cementite are related by the Bagaryatsky orientation relation. The corresponding example of the satisfiability of the Bagaryatsky orientation relation is shown in Figure 3.

According to the microdiffraction pattern (see Figure 3b) and its indexed pattern (see Figure 3c), cementite particles lie in the plane of the $(13\bar{2})$ α-phase foil, which is parallel to the plane $(1\bar{2}0)$ of cementite, i. e. $(13\bar{2})//(012)_C$. In these directions, $[112]_\alpha$ and $[001]_C$ are parallel, i. e. $[112]_\alpha//[001]_C$ (parallel directions of α-matrix and cementite are indicated by an arrow in the micro-diffraction pattern).

It is known [17] that the main process of tempering is the decomposition of martensite with the release of carbides. As a result, after tempering, the steel is actually a ferritic-carbide mixture. However, as shown by electron microscopic studies, the released material always contains boundaries inherited from the martensitic structure. Therefore, this structure is called tempered martensite [17].

It is highlighted once again that in all crystals of all the morphological components of martensite, cementite particles, first, are inside martensitic crystals, second, have two or three orientations and, third, have the same (lamellar) form. However, particle sizes, distribution density and volume fraction in different morphological components of martensite are different. This means that the largest particles and the largest volume fraction of cementite are in the plates of high-temperature martensite, the smallest particles and the smallest volume fraction of cementite are in the rack martensite. Quantitative estimates of cementite particles in various morphological components of α-martensite and on average of the material in the transition layer of nitro-cemented 18CrNi3Mo steel are given in Table 1.

Morphological component	Cementite particle sizes		Distance between the particles of cementite	Volume fraction of cementite
	d (nm)	l (nm)	r (nm)	δ (%)
Batch martensite	10	100	80	0.7
Lamellar low-temperature martensite	12	120	100	0.8
Lamellar high-temperature martensite	16	400	140	2.4
Average by material	13	210	110	1.3

Table 1: Sizes of cementite particles, the distances between them and the volume fractions of cementite in various morphological components of α-martensite and on average by material, transition layer of carbonitriding 18CrNi3Mo steel

Morphological component	Sizes of γ-phase interlayers		Volume fraction of γ-phase
	d (nm)	l (nm)	ΔVγ (%)
Batch martensite	12	600	2.0
Lamellar low-temperature martensite	8	800	1.5
Lamellar high-temperature martensite	-	-	0
Average by material	10	680	1.2

Table 2: Sizes of γ-phase interlayers and their volume fractions in various morphological components of α-martensite and on average by material, transition layer of carbonitriding 18CrNi3Mo steel

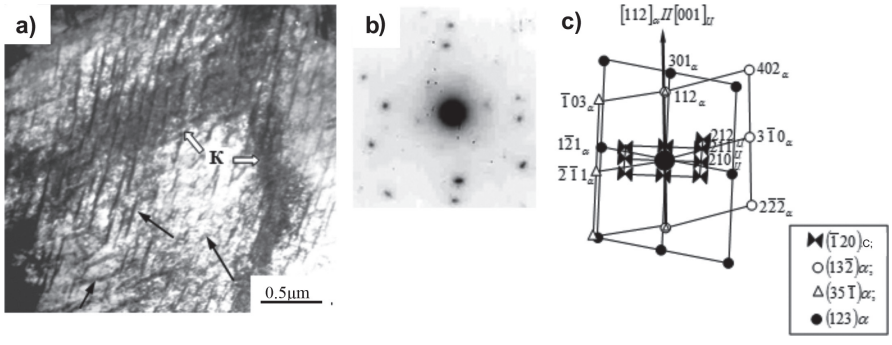

Figure 3: Intermediate layer of 18CrNi3Mo steel after carbonitriding, electron-microscopic image of the released high-temperature martensite, a) light-field image (arrows indicate cementite particles), b) microdiffraction pattern, c) indicated scheme, the arrow indicates the coinciding directions of α-phase and cementite [001], i. e. $[13\bar{2}]_\alpha // [\bar{1}20]_C$, while the ratio: (Bagaryatsky ratio), K: bending extinction contour

At the boundaries of martensitic rails and plates of low-temperature martensite, residual austenite is present in the form of thin long layers (see Figures 1 and 2). The crystal lattices of the α-phase and residual austenite are related by the Kurdyumov – Zaks orientation relations [18]. The existence of the Kurdyumov – Zaks ratio in Figure 1, on which the packet of martensitic rails is presented, is confirmed by the micro-diffraction pattern (see Figure 1c) and its scheme (see Figure 1d), from which it is clear that the direction $[001]_\alpha$ coincides with direction $[001]_\gamma$ (the coinciding directions in the micro diffraction pattern are indicated by an arrow), i. e. $[001]_\alpha//[001]_\gamma$ and $(010)_\alpha//(110)_\gamma$. The same conclusion follows when indexing microelectron diffraction patterns obtained from sections of the material containing low-temperature lamellar martensite. The corresponding example is shown in Figure 2. The indication of the microdiffraction pattern (see Figure 2c) shows that the direction $[110]_\alpha$ coincides with the direction $[010]_\gamma$. This means that these directions in the crystal lattices of the α- and γ-phases are parallel, i. e. $[110]_\alpha//[010]_\gamma$, as can be seen in the diagram (see Figure 2d). In this case, the planes are also parallel:$(\bar{1}10)_\alpha//001)_\gamma$. Exactly this one is obtained also from the solution of matrix equalities for the feasibility of the Kurdyumov – Zaks relation.

Quantitative assessment of the layers of residual austenite in various morphological components of α-martensite and, on average, the material in the transition layer of carbonitriding 18CrNi3Mo steel are given in Table 2.

It can be seen from the table that, firstly, the γ-phase interlayers in the batch martensite are coarser, but shorter than in the

lamellar low-temperature martensite. Second, the volume fraction of the γ-phase in the packet martensite is smaller. In crystals of high-temperature plate martensite, the γ-phase is completely absent. On average, the size of the interlayers is 10 × 680 nm, the volume fraction of the γ-phase is ~1.2 %.

There is another carbonitride phase, i. e. carbonitride $M_{23}(C,N)_6$, in addition to cementite, in the transition layer of carbonitride 18CrNi3Mo steel. Particles of this phase are especially clearly visible in dark-field images obtained in γ-phase reflections (see Figure 4). The crystal lattices of carbonitride $M_{23}(C,N)_6$. and γ-phases are connected by the orientation cube-cube relation. The feasibility of this ratio confirms the indexing of microdiffraction patterns obtained from such parts of the structure. One of the examples confirming the feasibility of this relationship is shown in Figure 4.

In the schematic presentation (see Figure 4d) of the displayed micro-diffraction pattern (see Figure 4c) it is clear that the direction of the γ-phase crystal lattice $[\bar{1}10]$ coincides with the direction in the crystal lattice of carbonitride $M_{23}(C,N)_6$, $[3\bar{1}0]$ i. e. //. In this case, the (112) γ-phase plane is parallel to the (131) plane of $M_{23}(C,N)_6$ carbonitride, i. e. $(112)_\gamma//(131)_K$ (here carbonitride $M_{23}(C,N)_6$ is designated as "K"). The same result is obtained when solving matrix equalities for the feasibility of the "cube – cube" relation.

Note that the carbonitride M23 $M_{23}(C,N)_6$ contains iron and chromium. Therefore, its chemical formula should be written as $(Fe,Cr)_{23}(C,N)_6$. Thus, chromium clearly manifests itself as a carbide-forming element, as in the case of cementite.

Besides the γ-phase, the $M_{23}(C,N)_6$ carbonitride particles are also inside the crystals of all the morphological components of martensite. These are small (d < 10 nm) round-shaped particles located in the nodes of dislocation networks. These particles are also clearly visible in dark-field images obtained in the reflections of this phase (see Figure 5).

Quantitative estimates made for carbonitride $M_{23}(C,N)_6$ in various morphological components of α-martensite and, on average, in the material in the transition layer of 18CrNi3Mo carbon steel are given in Table 3.

It can be seen from the table that particles of carbonitride $M_{23}(C,N)_6$ are mainly located at the boundaries of the morphological components of α-martensite. Inside the morphological components, the volume fraction of carbonitride $M_{23}(C,N)_6$ is small. Nevertheless, the presence of particles on dislocations cannot be ignored. The fact is that the rounded shape of the particles, their small size and small distance between them (and therefore high density of distribution) lead to a significant hardening of the material [19].

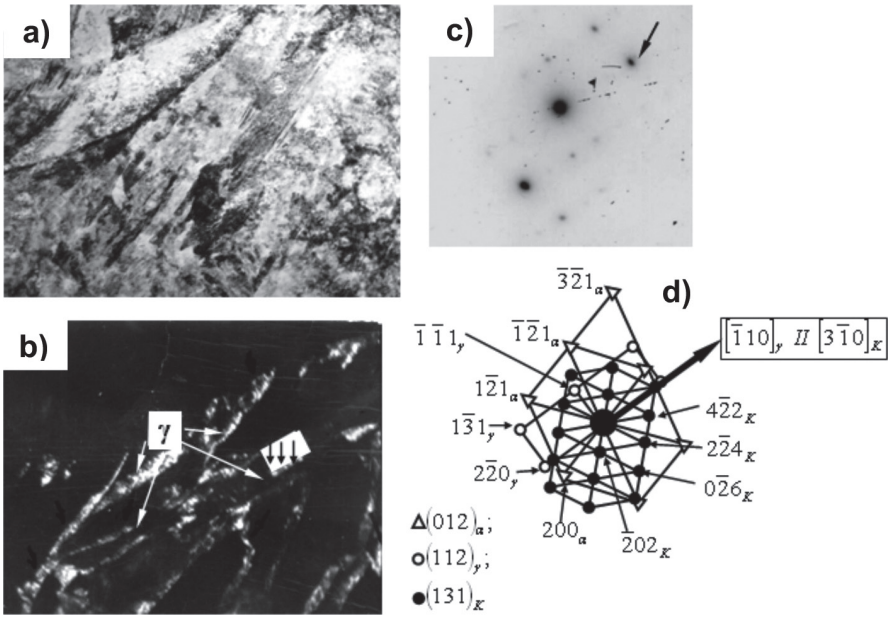

Figure 4: Selection of carbonitride $M_{23}(C,N)_6$ in the layers of residual austenite, electron-microscopic image, a) light-field image, b) dark-field image obtained in the coincident reflexes of reflexes $[\bar{2}20]_\gamma$ + $[6\bar{2}0]_K$, marked on the micro-diffraction pattern, c) microdiffraction pattern, d) indexed scheme, the arrow indicates the coinciding directions $[\bar{1}10]_\gamma$ u $[3\bar{1}0]_K$, which means $[\bar{1}10]_\gamma//[3\bar{1}0]_K$, – relations of "cube-cube"

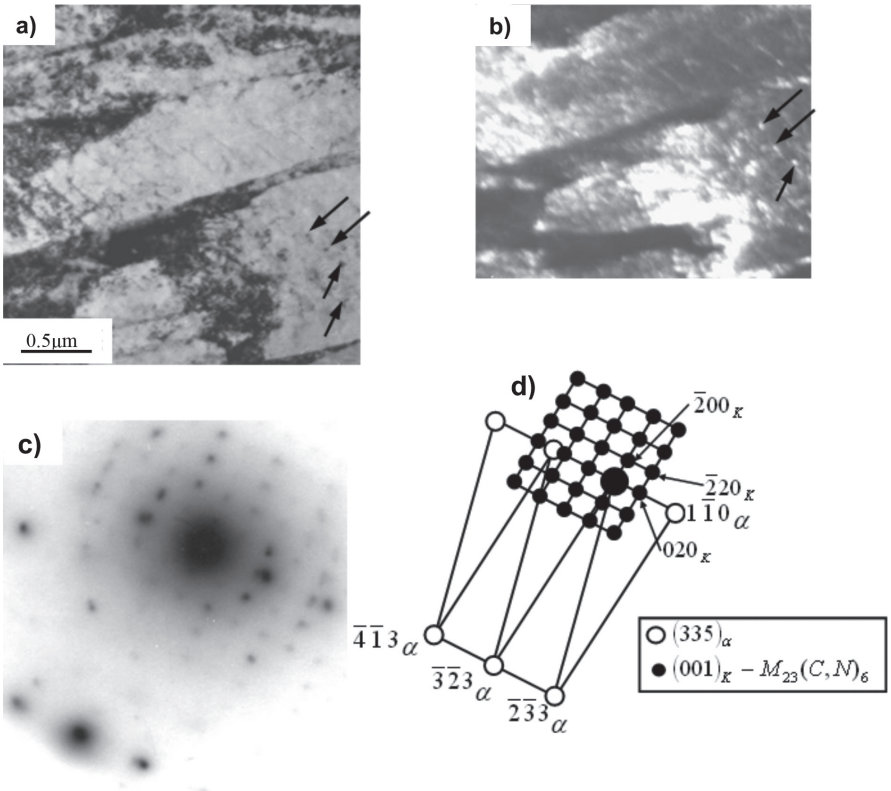

Figure 5: Carbonitride $M_{23}(C,N)_6$ on dislocations inside the α-phase crystals, a) light-field image, b) dark-field image obtained in the coincident reflexes $[040]_K + [1\bar{1}0]_\alpha$, c) microdiffraction pattern, d) indexed pattern (there are reflexes related to the (335) α-phase planes and (001) carbonitride $M_{23}(C,N)_6$, designated as "K"

Morphological component	Particle locations	Particle size		Volume fraction $M_{23}(C,N)_6$
		d (nm)	r (nm)	δ (%)
Batch martensite	inside	8	40	0.1
	on the boundaries	12	20	1.3
	in the batch	10	30	1.4
Lamellar low-temperature martensite	inside	12	60	0.2
	on the boundaries	10	20	0.97
	in the plate	11	40	1.0
Lamellar high-temperature martensite	inside	12	60	0.2
	on the boundaries	–	–	–
	in the plate	12	60	0.2
Average by material	inside	10	50	0.2
	on the boundaries	12	20	0.7
	In material	11	40	0.9

Table 3: Sizes of particles of carbonitride $M_{23}(C,N)_6$ and their volume fractions in various morphological components of α-martensite and on average by material, transition layer of nitrocemented 18CrNi3Mo steel

Conclusions

Based on the analysis of the obtained research results, we can draw the following conclusions:

- It was established that α-phase is tempered martensite after carbonitriding. Released martensite is represented by batch, or lath and lamellar low-temperature and high-temperature martensite.
- It is determined that the whole martensite is in the released state. It was also found that lamellar cementite precipitates are simultaneously present inside the tempered martensitic crystals.
- It was established that the residual austenite present at the boundaries of martensitic rails and plates of low-temperature martensite is coarser. However, it is shorter in batch martensite, but shorter than in low-temperature plate martensite.
- It is revealed that the particles of carbonitride $M_{23}(C,N)_6$ found in the transition layer of carbonitrided 18CrNi3Mo steel are located inside the crystals of all the morphological components of α-martensite. We can also draw a reasonable conclusion that the rounded shape of the particles of the carbonitride phase $M_{23}(C,N)_6$, their small size and small distance between them (and therefore a high distribution density) lead to significant hardening of the material.

Funding

This research was funded by the Science Committee of the Ministry of Education and Science of the Republic of Kazakhstan (Grant No. AP08857733).

References

1 I. Suminov, P. Belkin, A. Epelfeld, V. Lyudin, B. Crit, A. Borisov: Plasma electrolytic modification of the surface of metals and alloys, Technosphere 2 (2011), Moscow, Russia, pp. 512
2 B. Rakhadilov, M. Skakov, M. Scheffler: Microstructure and tribological properties of electrolyte plasma nitrided high speed steel, Materials Testing 57 (2015), pp. 360-365 DOI:10.3139/120.110709
3 A. Yerokhin, X. Nie, A. Leyland, A. Matthews, S. Dowey: Plasma electrolysis for surface engineering, Surface and Coating Technology 122 (1999), pp 73-93 DOI:10.1016/S0257-8972(99)00441-7
4 M. Bayati, R. Molaei, K. Janghorban: Surface alloying of carbon steels from electrolytic plasma, Metal Science and Heat Treatment 53 (2011), pp. 91-94 DOI:10.1007/s11041-011-9347-5
5 M. Skakov, L. Bayatanova, M. Scheffler: Examination of phase composition and mechanical properties of drilling tool material after electrolytic plasma treatment, Materials Testing 56 (2014), pp. 622-628 DOI:10.3139/120.110606
6 M. Skakov, G. Uazyrkhanova, N. Popova, M. Scheffler: Influence of deformation on the phase-structural state of a 30CrMnSiA steel, Materials Testing 55 (2013), pp. 51-54 DOI:10.3139/120.110404
7 L. Zhurerova, B. Rakhadilov, N. Popova, M. Kylyshkanov, V. Buraniche, A. Pogrebnjak: Effect of the PEN/C surface layer modification on the microstructure, mechanical and tribological properties of the 30CrMnSiA mild-carbon steel, Journal of Materials Research and Technology (2019), pp. 78-85 DOI:10.1016/j.jmrt.2019.10.057
8 A. Guriev, E. Kozlov, L. Ignatenko, N. Popova: Physical basis of thermocyclic boring of steel, Altai State Technical University, Barnaul, Russia (2000), pp. 216
9 A. Guriev, B. Lygdenov, N. Popova, E. Kozlov: Physical bases of chemical-thermocyclic processing of steels, Altai State Technical University, Barnaul, Russia, (2008), p. 256
10 N. Popova, L. Bayatanova, E. Nikonenko, M. Skakov, E. Kozlov: Phase composition and fine structure of 0.18C–1Cr–3Ni–1Mo–Fe steel after plasma-electrolytic treatment, AIP Conference Proceedings (2017), p. 030002 DOI:10.1063/1.4973034
11 M. Skakov, L. Bayatanova, M. Sheffler: Changes of structural-phase condition in 18CrNi3MoA-Sh steel after electrolyte-plasma processing, Advanced Materials Research 601 (2013), pp. 74-78 DOI:10.4028/www.scientific.net/AMR.601.74
12 M. Skakov, L. Bayatanova, N. Popova: TEM – Studies of the structure and phase composition of steel 18CrNi3Mo after exposure to electrolytic plasma, Bulletin of KazNTU, Physical and Mathematical Sciences Series 103 (2014), pp. 487-493
13 Yu. Ivanov, E. Kozlov: Multistep scheme of the martensitic transformation of low- and medium-carbon low-alloy steels, Materials Science 11 (2000), pp. 33-37, DOI ?
14 G. Krauss, A. Marder: The morphology of martensite in iron alloys, Metallurgical Transactions 2 (1971), pp. 2343-2357 DOI:10.1007/BF02814873
15 N. Koneva, L. Trishkina, T. Cherkasova: Evolution of Dislocation Structure Parameters in Deformed Polycrystalline FCC Solid Solutions, Russian Physics Journal 62 (2019), pp 948-955 DOI:10.1007/s11182-019-01800-1
16 N. Koneva, L. Trishkina, T. Cherkasova: Effect of stacking-fault energy on the accumulation of dislocations during plastic deformation of copper-based polycrystalline alloys, Letters on Materials 7(3) (2017), pp. 282-286 DOI:10.22226/2410-3535-2017-3-282-286
17 G. Kurdyumov, L. Utevsky, R. Entin: Transformations in iron and steel, Science, Moscow, Russia (1997), pp. 236
18 N. Ganina, A. Zakharov, V. Olenicheva, L. Petrova Diagrams of metallic systems, VINITI, Location ? (1991), pp. 368
19 N. Koneva, E. Kozlov: Dislocation structure and physical mechanisms of hardening of metallic materials, Perspective Materials 1 (2006), pp. 267-320

Bibliography

DOI 10.1515/mt-2020-0119
Materials Testing
63 (2021) 9, pages 842-847

ISSN 0025-5300, e-ISSN 2195-8572

The authors of this contribution

Dr. Lyaila Bayatanova was born in 1983, Kazakhstan. She studied Physics and Computer Science in

Sarsen Amanzholov East Kazakhstan State University in 2006, continued her education at Daulet Serikbaev East Kazakhstan State Technical University and received her master's degree in 2008, continuing her PhD at the same university since 2011. Her research interests lie in the physics of condensed state. She is a senior researcher of the Scientific Research Center "Surface Engineering and Tribology" by nonprofit limited company Sarsen Amanzholov East Kazakhstan University, Ust-Kamenogorsk, Kazakhstan.

Prof. Dr. Bauyrzhan Rakhadilov, born in 1988, studied physics and the mechanical properties of steel under thermal treatment at DauletSerikbaev East Kazakhstan Technical University, Kazakhstan. He began work at the university as a Scientific Assistant. His research is focused on the physics of condensed state, plasma technology, polymers and tribology research. He is a senior researcher of the Scientific Research Center "Surface Engineering and Tribology" by nonprofit limited company Sarsen Amanzholov East Kazakhstan University, Ust-Kamenogorsk, Kazakhstan.

Prof. Dr. Sherzod Kurbanbekov was born in 1988. He works at Khoja Akhmet Yassawi International Kazakh-Turkish University, department of physics. His research interests include the physics of condensed state, plasma technology and alternative energy forms. He has published more than 85 papers in refereed journals. He is currently an Associate Professor at the Khoja Akhmet Yassawi International Kazakh-Turkish University.

Prof. Dr. Mazhyn Skakov, born in 1952, studied the physics of condensed state, radiation physics of solid body and reactor material testing at the Tomsk Polytechnic Institute, Russia. He chaired the Research-Scientific Institute of Nanotechnologies and New Materials. He is Deputy R&D Director General of the Republican State Enterprise National Nuclear Center of the Republic of Kazakhstan, Kurchatov, Kazakhstan.

Prof. Dr. Natalia Popova, born 1952 in Russia, holds a Ph.D. in technical science. She is also a research assistant of the Tomsk state architecture and building university (Russia). Her research interests are focused on the physics of condensed state. She has published more100 papers in refereed journals.